AEgIS experiment: Towards antihydrogen beam production for antimatter gravity measurements*

Sebastiano Mariazzi[1,a], Stefano Aghion[2,3], Claude Amsler[4], Akitaka Ariga[4], Tomoko Ariga[4], Alexandre S. Belov[5], Germano Bonomi[6,7], Philippe Bräunig[8], Roberto S. Brusa[9], Johan Bremer[10], Louis Cabaret[11], Carlo Canali[12], Ruggero Caravita[2,13], Fabrizio Castelli[13], Giovanni Cerchiari[3,13], Simone Cialdi[13], Daniel Comparat[11], Giovanni Consolati[3,14], Luca Dassa[6], Jan Hendrik Derking[10], Sergio Di Domizio[15], Lea Di Noto[9], Michael Doser[10], Alexey Dudarev[10], Antonio Ereditato[4], Rafael Ferragut[2,3], Andrea Fontana[7], Pablo Genova[7], Marco Giammarchi[3], Angela Gligorova[16], Sergei N. Gninenko[5], Stephen D. Hogan[17], Stefan Haider[10], Elena Jordan[18], Lars V. Jørgensen[10], Thomas Kaltenbacher[10], Jiro Kawada[4], Alban Kellerbauer[18], Mitsuhiro Kimura[4], Andreas Knecht[10], Daniel Krasnický[15,19], Vittorio Lagomarsino[19], Sebastian Lehner[1], Chloe Malbrunot[1,10], Viktor A. Matveev[5,20], Frederic Merkt[21], Fabio Moia[2,3], Giancarlo Nebbia[22], Patrick Nédélec[23], Markus K. Oberthaler[8], Nicola Pacifico[16], Vojtech Petráček[24], Ciro Pistillo[4], Francesco Prelz[3], Marco Prevedelli[25], Christian Regenfus[12], Cristina Riccardi[7,26], Ole Røhne[27], Alberto Rotondi[7,26], Heidi Sandaker[16], Paola Scampoli[4,28], James Storey[4], Martin A. Subieta Vasquez[6,7], Michal Špaček[24], Gemma Testera[15], Renzo Vaccarone[15], Fabio Villa[13], Eberhard Widmann[1], Sandra Zavatarelli[15], and Johann Zmeskal[1]

[1] Stefan-Meyer-Institut für subatomare Physik, Boltzmanngasse 3, 1090 Vienna, Austria
[2] Politecnico di Milano, LNESS and Dept of Physics, Via Anzani 42, 22100 Como, Italy
[3] Istituto Nazionale di Fisica Nucleare, Sez. di Milano, Via Celoria 16, 20133 Milano, Italy
[4] Albert Einstein Center for Fundamental Physics, Laboratory for High Energy Physics, University of Bern, 3012 Bern, Switzerland
[5] Institute for Nuclear Research of the Russian Academy of Sciences, 117312 Moscow, Russia
[6] University of Brescia, Dept of Mech. and Indust. Engineering, Via Branze 38, 25133 Brescia, Italy
[7] Istituto Nazionale di Fisica Nucleare, Sez. di Pavia, Via Agostino Bassi 6, 27100 Pavia, Italy
[8] University of Heidelberg, Kirchhoff Institute for Physics, Im Neuenheimer Feld 227, 69120 Heidelberg, Germany
[9] Department of Physics, University of Trento and INFN TIFPA, Via Sommarive 14, 38123 Povo, Trento, Italy
[10] European Organisation for Nuclear Research, Physics Department, 1211 Genève 23, Switzerland
[11] Laboratoire Aimé Cotton, CNRS, Université Paris Sud, ENS Cachan, Bâtiment 505, Campus d'Orsay, 91405 Orsay Cedex, France
[12] University of Zurich, Physics Institute, Winterthurerstrasse 190, 8057 Zürich, Switzerland
[13] University of Milano, Dept of Physics, Via Celoria 16, 20133 Milano, Italy
[14] Politecnico di Milano, Dept of Aerospace Sci. and Tech., Via La Masa 34, 20156 Milano, Italy
[15] Istituto Nazionale di Fisica Nucleare, Sez. di Genova, Via Dodecaneso 33, 16146 Genova, Italy
[16] University of Bergen, Institute of Physics and Technology, Alleegaten 55, 5007 Bergen, Norway
[17] University College London, Dept of Physics and Astronomy, Gower Street, London WC1E 6BT, UK
[18] Max Planck Institute for Nuclear Physics, Saupfercheckweg 1, 69117 Heidelberg, Germany
[19] University of Genoa, Dept of Physics, Via Dodecaneso 33, 16146 Genova, Italy
[20] Joint Institute for Nuclear Research, 141980 Dubna, Russia
[21] ETH Zurich, Laboratory for Physical Chemistry, 8093 Zürich, Switzerland
[22] Istituto Nazionale di Fisica Nucleare, Sez. di Padova, Via Marzolo 8, 35131 Padova, Italy
[23] Claude Bernard University Lyon 1, Institut de Physique Nucléaire de Lyon, 4 rue Enrico Fermi, 69622 Villeurbanne, France
[24] Czech Technical University in Prague, FNSPE, Bøehová 7, 11519 Praha 1, Czech Republic
[25] University of Bologna, Dept of Physics, Via Irnerio 46, 40126 Bologna, Italy
[26] University of Pavia, Dept of Nuclear and Theoretical Physics, Via Bassi 6, 27100 Pavia, Italy
[27] University of Oslo, Dept of Physics, Sem Sælands vei 24, 0371 Oslo, Norway
[28] University of Napoli Federico II, Department of Physics, Via Cinthia, 80126 Napoli, Italy

Received 4 November 2013 / Received in final form 17 December 2013 Published online 4 March 2014

* Contribution to the Topical Issue "Electron and Positron Induced Processes", edited by Michael Brunger, Radu Campeanu, Masamitsu Hoshino, Oddur Ingólfsson, Paulo Limão-Vieira, Nigel Mason, Yasuyuki Nagashima and Hajime Tanuma.

[a] e-mail: mariazzi@science.unitn.it

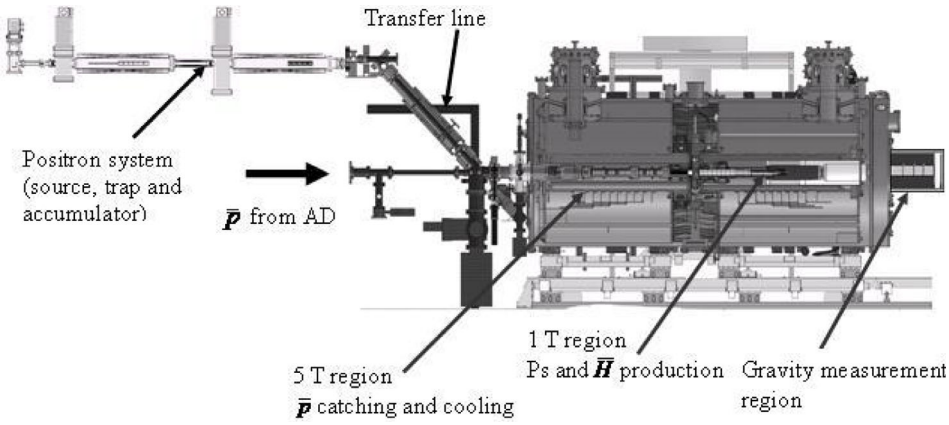

Fig. 1. Schematic view of the AEgIS apparatus.

1 Introduction

The weak equivalence principle (WEP) states that the trajectory of a body solely under the influence of gravity is independent of the composition and internal structure of the body itself. The universality of free fall has been tested with a precision of parts in 10^{-13} by using probes of various materials [1] but it has never been tested with antimatter particles. Heretofore, the main limit for WEP tests with antimatter was the challenge to reduce electromagnetic disturbances to a level such that the effect of the much weaker gravitational force could be observed. Production of antihydrogen ($\overline{H}$), achieved for the first time in 2002 [2,3], opened the possibilities to perform tests of the WEP with electrically neutral antimatter atoms.

The main scientific goal of AEgIS is the direct measurement of the gravitational acceleration g on antihydrogen in the Earth's field [4]. The gravitational measurement in AEgIS will be performed by forming a pulsed cold antihydrogen beam and by observing its vertical displacement after passing through a moiré deflectometer [5]. The essential steps leading to the production of a cold $\overline{H}$ beam and the measurement of its gravitational interaction are the following: (1) accumulation of positrons (e^+) in a Surko-type trap + Penning-Malmberg accumulator (First Point scientific technology) [6]; (2) capture and accumulation of antiprotons ($\overline{p}$) delivered by Antiproton Decelerator (AD) at CERN; (3) cooling of the $\overline{p}$ cloud to sub-K temperatures. $\overline{p}$ trapping and cooling will occur in a cylindrical Penning-Malmberg trap; (4) production of a cold positronium (Ps) cloud by injection of an intense e^+ pulse in a nanoporous material kept at cryogenic temperature; (5) two-step laser excitation of Ps to a Rydberg state (Ps^*) with principal quantum number n between 20 and 30 [7]; (6) formation of cold Rydberg antihydrogen ($\overline{H}^*$) by charge exchange reaction [8]: $\overline{p} + Ps^* \rightarrow \bar{H}^* + e^+$; (7) formation of $\overline{H}$ beam by Stark acceleration with inhomogeneous electric fields; (8) measurement of the vertical deflection of the beam due to its free fall in a two-grating moiré deflectometer coupled with a position-sensitive detector.

The charge exchange reaction has a cross section up to 10^{-8} cm^2 provided that two conditions are satisfied: Ps has to be exited in a Rydberg state with $n > 20$ and Ps velocity has to be lower than the orbital e^+ speed in the Ps Rydberg atom. If $n > 20$, a Ps velocity of few 10^4 m/s is required. The $\overline{H}$ will be produced in a Rydberg state and with a low velocity (25–80 m/s) if $\overline{p}$ are cooled to sub-K temperatures. An electric field gradient can be then applied in order to accelerate $\overline{H}$ to ∼400 m/s and generate the beam. This manipulation technique has already been demonstrated with hydrogen atoms by members of the AEgIS collaboration [9].

2 Apparatus design

Figure 1 shows a scheme of the AEgIS apparatus. A bunch of typically 3×10^7 $\overline{p}$ at 5.3 MeV energy will be delivered every 120 s from AD. $\overline{p}$, slowed down in a set of thin aluminum foils (degrader foils), are injected into a 5 T magnet where they are caught in a cylindrical Penning-Malmberg trap with an internal radius of 1.5 cm. The trapping is achieved by raising a first high voltage electrode (HV1) at the entrance of the trap after the passage of the antiproton bunch. A second high voltage electrode (HV2) placed 46 cm downstream of the first one is used to catch $\overline{p}$. A third high voltage electrode (HV3) can be used in order to increase the trapping length to 76 cm. Trapped antiprotons will be subsequently cooled down to sub-eV energy by a cloud of 10^7–10^8 electrons loaded into a 100–150 eV deep potential well before the antiproton arrival. By interaction with electrons, trapped antiprotons remain confined in the 100–150 eV well. After cooling, antiprotons will be transferred in a 1 T magnet where they will be trapped in a second Penning-trap mounted in a 100 mK region (Fig. 2).

In this second Penning-trap, $\overline{p}$ can react with Ps^* that is produced as explained in the following. Positrons emitted by a ^{22}Na radioactive source are slowed by a solid Ne moderator. Subsequently e^+ are cooled by interaction with N_2 gas and trapped in a buffer gas trap (Surko-trap) [6]. Several times per second, bunches of 10^4–10^5 e^+

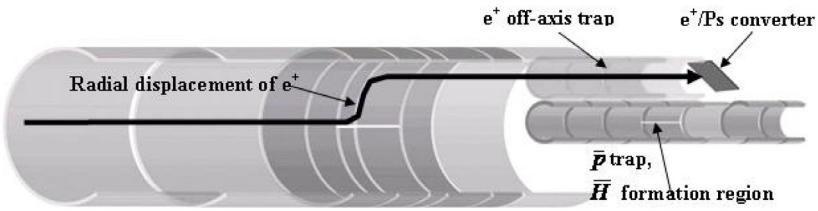

Fig. 2. Schematic of the region where antihydrogen will be produced. The positron cloud is loaded into a high voltage off-axis trap by excitation of the diocotron mode of the plasma whereas antiprotons are transferred along the axis to the ultracold trap.

are transferred from the trap to a Penning-Malmberg accumulator where up to 10^8 positrons can be accumulated in some tens of seconds. Bunches of 10^8 e^+ can be released from the accumulator and magnetically guided in the 5 T magnet, and successively transferred in the 1 T magnet. Here positrons are trapped in a large radius Penning-Malmberg trap located along the main-axis (Fig. 2) moved off-axis by excitation of the diocotron mode of the plasma [10] and then loaded in an off-axis high voltage trap before being accelerated towards the e^+/Ps conversion target.

The target will be a nanoporous based silica sample. In particular a Si target, in which ordered oxidized nanochannels where produced perpendicular to the surface, is planned to be used [11,12]. In this materials Ps is formed efficiently and emitted into the channels with an energy of a few eV. Formed Ps reduces its kinetic energy by collisions with the walls of the channels and a fraction can escape into vacuum with the required velocity of few 10^4 m/s [12] if the sample is held at low temperature. After emission into the vacuum, Ps will be excited to a Rydberg state [7]. A two-step laser excitation will be used for the transition from the ground state to $n = 3$ state (by an UV laser with wavelength $\lambda = 205$ nm) and from $n = 3$ to Rydberg state (by IR laser $\lambda \sim 1670$ nm) [13]. Laser will be injected in the 1 T region and transported to the antihydrogen production region via glass fibres and prisms.

After excitation, Ps atoms will enter through a semi-transparent electrode in the Penning-trap where $\overline{p}$ are trapped and Rydberg $\overline{H}$ atoms will be produced with an estimated rate of around 10 per $\overline{p}$ shot. The semi-transparent electrode has a beehive structure optimized to allow the passage of the maximum number of Ps atoms while maintaining a good harmonicity of the Penning-trap. Produced antihydrogen will be accelerated by the Stark effect and it will pass the moiré deflectometer [5]. This device is composed by two gratings separated by a distance $L \sim 50$ cm and a position-sensitive detector placed at the same distance L from the second grating (Fig. 3). The two gratings create a pattern of $\overline{H}$ annihilations on the detector (moiré intensity pattern). The gravity force on antihydrogen will induce a vertical displacement Δx of the moiré fringe pattern:

$$\Delta x = -gL^2/v^2 \qquad (1)$$

where g is the gravitational acceleration on $\overline{H}$ and v is the beam velocity. By measuring Δx with the position-sensitive detector and the beam time of flight (and thus its velocity) the local gravitational acceleration of antihydrogen g can be achieved by using equation (1).

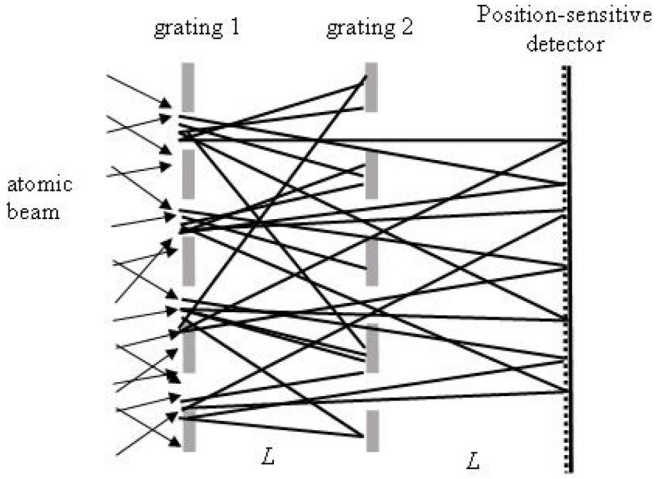

Fig. 3. Schematic of the moiré deflectometer composed of two gratings and the position sensitive detector.

In order to determine g with a precision of 1%, the detection of the annihilation point of about 10^3 antihydrogen atoms is required with a svertical precision of 1 μm. Several types of detector are under investigation to reach this high resolution in vacuum and under cryogenic conditions [14,15].

3 Status and commissioning of the apparatus: the positron, antiproton and laser systems

During 2012, many parts of AEgIS system have been assembled and commissioned. In Figure 4, a picture of the apparatus in November 2012 is shown.

Both 5 T and 1 T magnets have been installed in the experimental zone along with the traps. Antiproton catching and cooling in the 5 T Penning-Malmberg trap has been tested during the two beam times in 2012 (May-June and November-December). A set of plastic scintillators coupled to magnetically shielded photomultiplier tubes were positioned around the 5 T and 1 T cryostat vessels and used to detect antiproton annihilations. The detection efficiency for single antiproton annihilation has been calculated using GEANT3 MC taking into account the real geometry of the apparatus. In Figure 5, the number of trapped antiprotons as a function of HV1 = HV2

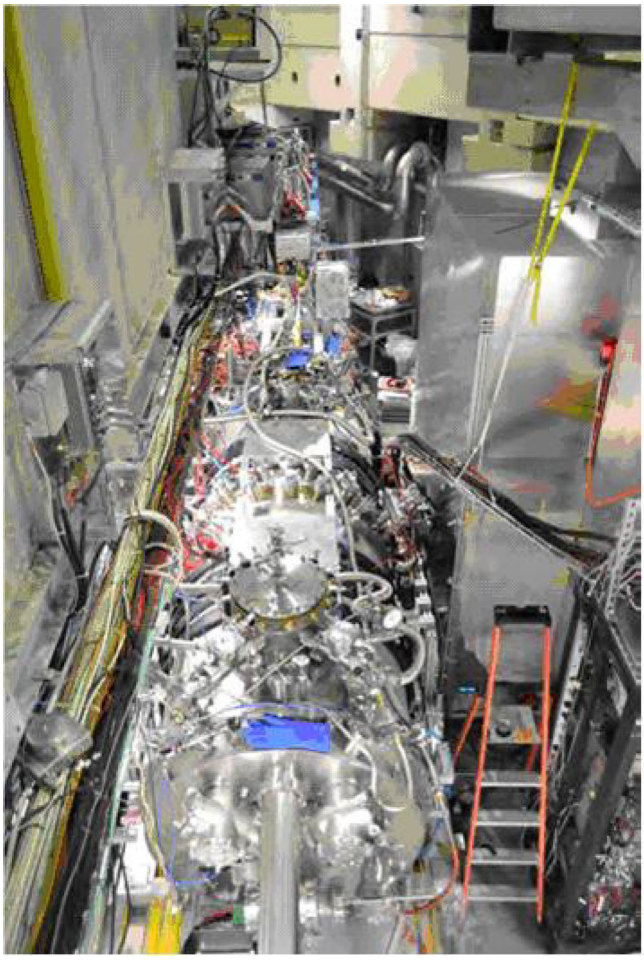

Fig. 4. Picture of the apparatus in November 2012.

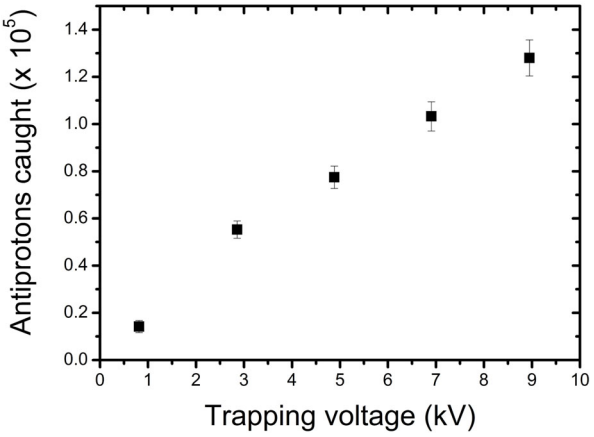

Fig. 5. Number of caught antiprotons vs. trapping voltage for 3.1×10^7 antiprotons in each AD bunch. Antiprotons were confined for 5 s in the 46 cm-long high voltage trap before being allowed to annihilate on the degrader foil.

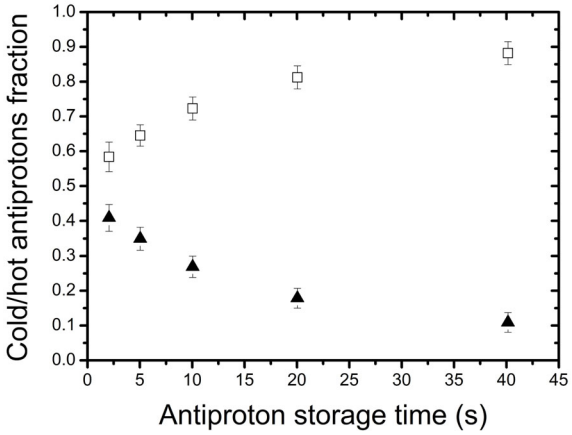

Fig. 6. Fraction of hot (full triangles) and cold (open squares) antiprotons as a function of the interaction time with electrons. Trapping voltage set at 9 keV.

potential are shown. $\overline{p}$ were stored for 5 s and then HV1 was switched off. Thus, $\overline{p}$ were allowed to annihilate on the degrader foil (so-called hot dump). By setting high voltage at 9 keV, $\sim 1.3 \times 10^5$ antiprotons were caught per AD bunch.

If a cloud of 10^7–10^8 electrons is previously loaded in the trap into a deep 100–150 eV deep potential well, a fraction of $\overline{p}$ loses its energy by collisions with electrons and remains confined in the same well. After the hot dump (obtained by switching off HV1) the cold dump can be performed by filling the potential well and releasing $\overline{p}$ towards the degrader foil. Cold and hot antiproton fractions as a function of the cooling time are shown in Figure 6. Measurement points out that ∼90% of antiprotons are cooled to eV-range in ∼40 s.

In 2012, the assembling and the test of positron system and transfer line have been successfully carried out. Fast positrons, produced by a ^{22}Na source with an activity of 16 mCi, have been converted to e^+ with energy of few eV by the using of a solid Ne moderator. The slow positrons have been guided by magnetic fields to the buffer gas trap. The efficiency of moderation and transport has been estimated by a set of calibrated CsI detectors coupled to photomultipliers to be $\sim 2.5 \times 10^{-3}$. In the Surko-trap, positrons have been cooled by interaction with N_2 gas, trapped and released every 0.15 s. The number of positrons in each dump has been estimated to be 5–6 $\times 10^4$ by using a second set of CsI detectors coupled to photodiodes. The trapping/dumping efficiency, calculated as the ratio between positrons injected in the trap and dumped positrons, resulted 0.14. Positrons released from the trap have been magnetically transported to the accumulator, where thanks to the low base pressure (5×10^{-10} mbar), many positron pulses can be stored for several hundreds of seconds. Positron storing occurs in a 12–15 eV deep harmonic potential well. The e^+ radial confinement in the accumulator is given by a 700 G magnetic field B generated by a high quality solenoidal magnet coil ($\Delta B/B \sim 10^{-4}$) built and tested at the Budker Institute of Nuclear Physics of Novosibirsk. In Figure 7 the number of positrons stored in the accumulator as a function of number of pulses from the trap (and thus as a function of time) are shown. In this test, up to 3×10^7 positrons have been stored in 330 s. The positron lifetime

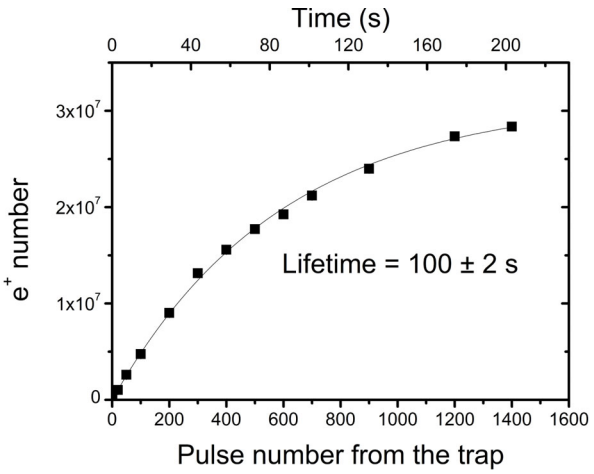

Fig. 7. Number of positrons stored in the accumulator vs. number of pulses from the trap. The reported positron lifetime has been calculated by fitting the experimental curve with an exponential function.

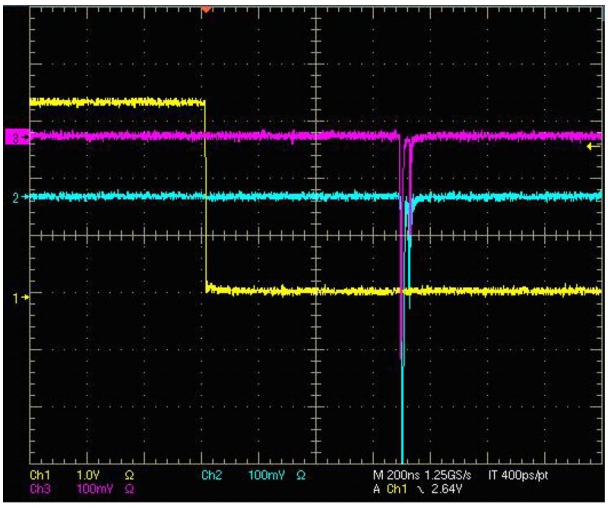

Fig. 8. Annihilation pulse of positrons arriving in the 1 T magnet as detected by two scintillators placed around the 1 T magnet respectively below (violet curve) and above (cyan curve) the annihilation region. Yellow line is the accumulator extraction trigger.

in the accumulator was around 100 s. This test has been performed by storing positrons for a given time and then bunching e^+ that were allowed to annihilate on a stopper placed at the exit of accumulator. Emitted annihilation gamma rays were detected by a calibrated CsI detector coupled to photodiodes in order to achieve the absolute positron number.

The positron bunch has been then extracted from the accumulator by the 0.1 T magnetic field of the transfer line and injected in the 5 T region along the axis of the trap. Thus the e^+ bunch was able to cross the 5 T and reach the 1 T region where positrons were allowed to annihilate. In Figure 8, the annihilation pulse of positrons arriving in the 1 T magnet detected by the scintillators placed around the 1 T magnet is shown.

Several porous materials have been synthesized and tested to fulfill the AEgIS experimental requirement of a large positron/slow Ps conversion. This has succeeded in producing a novel target of silicon in which ordered nanochannels were realized by electrochemical etching and successively oxidized [11,12]. This novel procedure has allowed tuning the size of the nanochannels from 4 to 100 nm. The possibility to tune the nanochannels size is important for achieving cold Ps because the minimum temperature reachable by Ps in a channel depends on its dimension due to the quantum confinement [16,17]. The minimal reachable Ps temperature is expected to lie between 116 K (for channels with size of 5 nm) and 7 K (for channels with size of 50 nm). Measurements with a Time of Flight Apparatus have provided first evidence of Ps cooling and thermalization below room temperature [12].

The laser system has been assembled, tested [13] and installed at CERN in October 2012. Both UV and IR pulsed-laser for the Ps excitation to Rydberg states are pumped by the same 650 mJ Q-switched Nd:YAG laser delivering a 4 ns pulse. The two wavelengths are produced through second-order polarization in optical crystals. The UV 205 nm radiation is obtained by summing in a non-linear BBO crystal the 266 nm fourth harmonic of the 1064 nm Nd:YAG pulse and the OPA-amplified 894 nm radiation generated in an optical parametric generator (OPG) by down-conversion of the second harmonic of the same laser. The IR wavelength (around 1670 nm) is generated in a single step by an OPG starting from the same pump laser and then amplified by a second optical parametric amplifier (OPA) system (Fig. 9). The energy required to saturate the transition to $n = 3$ and from 3 to Rydberg states is 32 μJ and 350 μJ, respectively. Both the required saturation powers have been exceeded. An energy of 250 μJ for the UV laser has been reached with an input energy of the Nd:YAG of 10 mJ at 266 nm. For the IR laser, an energy of 3 mJ has been reached using a Nd:YAG laser of only 80 mJ per pulse.

Laser light for Ps excitation has been injected in the 1 T region and transported to the antihydrogen production region via glass fibres (for IR laser) and prisms (for UV laser). The whole chain has been aligned. The stability of the alignment during the cool down of the apparatus and the possibility to externally adjust residual misalignments by optimizing the path taken by the laser on the laser table have been verified.

4 Short term plans and conclusions

Since antiprotons are not available during 2013 and part of 2014 due to shut down of accelerator complex at CERN, we are focusing our attention on Ps formation and Ps laser excitation. A new flexible chamber has been designed and constructed to match the AEgIS positron system and it is in phase of installation at the end of the positron accumulator, above the transfer section (for a detailed description see Ref. [18]). This new chamber is comprised of a line to transport the e^+ bunch from the exit of the accumulator

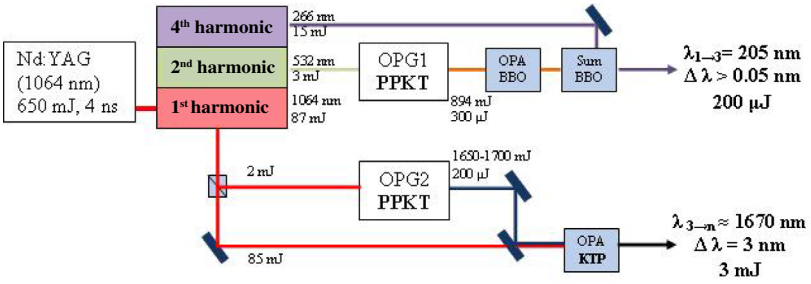

Fig. 9. Schematic of the laser system for the Rydberg excitation of Ps.

and to inject the e^+ into the e^+/Ps converter in few ns and with an energy tuneable between 5 and 8 keV. Fast switches are used to raise the electrodes of a buncher up to 8 keV and set in 3–5 ns the parabolic potential that compresses and accelerates the bunch on the sample. Simulations of the device have shown that achieving pulses of less than 5 ns and localized in less than 3–4 mm is feasible with this set-up. The positron/Ps converter is placed in a chamber with a number of ports for UV and IR lasers, vacuum equipment, instrumentation and detector feedthroughs. A cryo-cooler gives the possibility to lower the target temperature to a few K.

In order to detect the transition $n = 1 \rightarrow 3$, Ps will be excited in a 100 Gauss magnetic field. In presence of this field, the long-lived Ps triplet state fraction excited to $n = 3$ with quantum number $m = 0$, can decay into the short-lived singlet ground state (quenching). The expected increase in the Ps annihilation rate at the laser pulse will be detected by using fast detectors such as the Cherenkov radiator PbF_2 [19]. The field ionization technique will be used to verify excitation to Rydberg states. In the next months the first test of excitation will be performed while for the future other experiments such as motional Stark effect studies [20], tests of Ps laser cooling [21] and study of Ps emission angular distribution have been proposed.

Moreover, efforts are under way to increase the positron lifetime in the accumulator (and thus the number of stored positrons) by improving the base pressure in the system and optimizing the alignment of magnetic axes of the trap and the accumulator. Dedicated correction coils have been installed and are under testing. Finally, we are commissioning the capture of the positron bunch in the 1 T trap and the loading of the high voltage off-axis trap by excitation of the diocotron mode.

In conclusion, the main part of AEgIS apparatus has been completed. In the first runs with antiprotons, the 5 T and 1 T superconducting magnets and the antiproton catching trap in 5 T region have been successfully tested. Test of positron storage in the accumulator and positron transport in the transfer line have been profitably performed as well as the laser tests and alignment. Further efforts are underway to increase the positron bunch intensity, to realize the first two-step laser excitation from the ground state to the $n = 3$ state and then to the Rydberg band and to optimize the e^+/Ps converter. These experiments are preparatory to produce the first $\overline{H}$ beam by the charge exchange reaction and to perform the first measurement of matter-antimatter gravitational interaction.

References

1. E.G. Adelberger, J.H. Gundlach, B.R. Heckel, S. Hoedl, S. Schlamminger, Prog. Part. Nucl. Phys. **62**, 102 (2009)
2. M. Amoretti et al. (ATHENA collaboration), Nature **419**, 456 (2002)
3. G. Gabrielse et al. (ATRAP collaboration), Phys. Rev. Lett. **89**, 213401 (2002)
4. A. Kellerbauer et al., Nucl. Instrum. Methods Phys. Res. B **266**, 351 (2008)
5. M.K. Oberthaler, S. Bernet, E.M. Rasel, J. Schmiedmayer, A. Zeilinger, Phys. Rev. A **54**, 3165 (1996)
6. R.G. Greaves, C.M. Surko, Phys. Rev. Lett. **85**, 1883 (2000)
7. D.B. Cassidy, T.H. Hisakado, H.W.K. Tom, A.P. Mills Jr., Phys. Rev. Lett. **108**, 043401 (2012)
8. M. Charlton, Phys. Lett. A **143**, 143 (1990)
9. E. Vliegen, F. Merkt, Phys. Rev. Lett. **97**, 033002 (2006)
10. J.R. Danielson, T.R. Weber, C.M. Surko, Phys. Plasmas **13**, 123502 (2006)
11. S. Mariazzi, P. Bettotti, S. Larcheri, L. Toniutti, R.S. Brusa, Phys. Rev. B **81**, 235418 (2010)
12. S. Mariazzi, P. Bettotti, R.S. Brusa, Phys. Rev. Lett. **104**, 243401 (2010)
13. S. Cialdi, I. Boscolo, F. Castelli, F. Villa, G. Ferrari, M.G. Giammarchi, Nucl. Instrum. Methods Phys. Res. B **269**, 1527 (2011)
14. S. Aghion et al., JINST **8**, P08013 (2013)
15. D. Fabris et al., Nucl. Phys. A **834**, 751 (2010)
16. S. Mariazzi, A. Salemi, R.S. Brusa, Phys. Rev. B **78**, 085428 (2008)
17. D.B. Cassidy, P. Crivelli, T.H. Hisakado, L. Liszkay, V.E. Meligne, P. Perez, H.W.K. Tom, A.P. Mills Jr., Phys. Rev. A **81**, 012715 (2010)
18. L. Penasa, L. Di Noto, M. Bettonte, S. Mariazzi, G. Nebbia, R.S. Brusa, J. Phys.: Conf. Ser., in press
19. D.B. Cassidy, A.P. Mills Jr., Nucl. Instrum. Methods Phys. Res. B **580**, 1338 (2007)
20. F. Castelli, Eur. Phys. J. Special Topics **203**, 137 (2012)
21. T. Kumita, T. Hirose, M. Irako, K. Kadoya, B. Matsumoto, K. Wada, N.N. Mondal, H. Yabu, K. Kobayashi, M. Kajita, Nucl. Instrum. Methods Phys. Res. B **192**, 171 (2002)